Preparation and Characterization of $Me_2O_3-CeO_2$ (Me = B, Al, Ga, In) Mixed-Oxide Catalysts

T. Yuzhakova,[†] V. Rakić,[†,‡] C. Guimon,[§] and A. Auroux*[,†]

IRCELYON, Institut de Recherches sur la Catalyse et l'Environnement de Lyon, UMR5256 CNRS−Université Lyon I, 2 Avenue Einstein, 69626 Villeurbanne Cedex, France, Faculty of Agriculture, Department of Chemistry, University of Belgrade, Nemanjina 6 11080 Zemun, Serbia, and IPREM−ECP, UMR 5254, Université de Pau et des Pays de l'Adour, 2 Avenue P. Angot, 64053 Pau Cedex 9, France

Received December 8, 2006. Revised Manuscript Received March 27, 2007

The present work is focused on the synthesis and characterization of ceria-based mixed oxides. Ceria was combined with the other oxides from group III, with the intention of improving the catalytic properties of thus obtained materials. (B_2O_3, Al_2O_3, Ga_2O_3, In_2O_3)−CeO_2 mixed oxides with a wide range of Me_2O_3 contents have been prepared by a coprecipitation route. The obtained solid materials have been characterized in terms of their structural, textural, and surface properties, including the acid−base and red−ox features, by a variety of techniques (BET, XRD, Raman, SEM, TG, TPR-TPO). The acid−base properties were estimated by the adsorption of probe molecules (NH_3 and SO_2), investigated by the use of two techniques: microcalorimetry and XPS. The obtained materials exhibited satisfactory homogeneity; the highest surface areas were achieved for $Al_2O_3-CeO_2$ mixed oxides. Only the fluorite structure of CeO_2 was observed by XRD for all prepared mixed oxides, along with the presence of oxygen vacancies, which has been proven by Raman spectroscopy. Red−ox properties were investigated for $In_2O_3-CeO_2$ samples. The degree of reduction decreased with In_2O_3 loading. Besides, the reduction−oxidation cycle, performed up to 830 °C, changed the morphology and structure of the samples irreversibly, leading to crystallization of In_2O_3. Among all investigated materials, only boria created significant acidity, whereas the basicity has been found to be dependent on the nature and amount of group III metal.

1. Introduction

Ceria and ceria-based materials have been probed for many different applications in a variety of fields: CeO_2 is included in materials used in fuel-cell processes,[1−11] in oxygen permeation membrane systems,[12−15] and as catalysts in numerous economically and technologically important industrial processes. Their use in the domain of catalysis is on the basis of superior chemical and physical stability, high oxygen mobility, and high oxygen vacancy concentrations, which are characteristics of fluorite-type oxides. The possibility of cycling easily between reduced and oxidized states ($Ce^{3+} \leftrightarrow Ce^{4+}$) permits the reversible addition and removal of O_2 from the CeO_2.[16−23] All mentioned features explain the applicability of these materials as promoters in fluid catalytic cracking processes (FCC)[24] or as an active component of three-way catalysts (TWC) for environmental purposes;[16−18,24−28] as well as their use in several groups of emerging catalytic processes: the oxidation of different

* Corresponding author. E-mail: aline.auroux@ircelyon.univ-lyon1.fr.
[†] Université Lyon 1.
[‡] University of Belgrade.
[§] Université de Pau et des Pays de l'Adour.

(1) Shao, Z.; Halle, S. M. *Nature* **2004**, *431*, 170.
(2) Laosiripojana, N.; Assabumrungrat, S. *Appl. Catal., B* **2005**, *60*, 107.
(3) Ramirez-Cabrero, E.; Atkinson, A.; Chadwick, D. *Appl. Catal., B* **2005**, *47*, 127.
(4) Ramirez-Cabrero, E.; Laosiripojana, N.; Atkinson, A.; Chadwick, D. *Catal. Today* **2003**, *78*, 433.
(5) Wong, F-Y.; Wan, B-Z.; Cheng, S. *J. Solid State Electrochem.* **2005**, *9*, 168.
(6) Wong, F-Y.; Chen, S.; Wang, Q.; Yuand, S.; Cheng, S. *Catal. Today* **2004**, *97*, 189.
(7) Panzero, G.; Madafferi, V.; Candamano, S.; Donato, A.; Frusteri, F.; Antonucci, P. L. *J. Power Sources* **2004**, *135*, 177.
(8) Sato, K.; Hashida, T.; Yashiro, K.; Yugami, H.; Kawada, T.; Mizusaki, J. *J. Ceram. Soc. Jpn.* **2005**, *113*, 562.
(9) Minh, N. Q. *J. Am. Ceram. Soc.* **1993**, *76*, 563.
(10) Kumar, A.; Devi, P. S.; Maiti, H. S. *Chem. Mater.* **2004**, *16*, 5562.
(11) Shanwen, T.; Jonh, T. S. I. *Chem. Mater.* **2004**, *16*, 4116.
(12) Kharton, V. V.; Kovalevsky, A. V.; Viskup, A. P.; Shaula, A. L.; Figueiredo. F. M.; Naumovich, E. N.; Marques, F. M. B. *Solid State Ionics* **2003**, *160*, 247.
(13) Levy, C.; Guizard. C.; Julbe, A. *Sep. Purif. Technol.* **2004**, *32*, 327.
(14) Yin, X.; Hong, L.; Liu, Z-L. *Appl. Catal., A* **2006**, *300*, 75.
(15) Yin, X.; Hong, L.; Liu, Z-L. *J. Membr. Sci.* **2006**, *268*, 2.
(16) Damyanova, S.; Bueno, J. M. C. *Appl. Catal., A* **2003**, *253*, 135.
(17) Ozaki, T.; Masui, T.; Machida. K.-I.; Adachi, G-Y.; Sakata, T.; Mori, H. *Chem. Mater.* **2000**, *12*, 643.
(18) Aneggi, E.; de Leitenburg, C.; Dolcetti, G.; Trovarelli, A. *Catal. Today* **2006**, *114*, 40.
(19) Zhao, S.; Gorte, R. K. *Appl. Catal., A* **2004**, *277*, 129.
(20) Wang, S.; Lu, G. Q. *Appl. Catal., B* **1998**, *19*, 267.
(21) He, H.; Dai, H.; Au, C. T. *Catal. Today* **2004**, *90*, 245.
(22) Reddy, B.; Khan, A.; Yamada, Y.; Kobayashi, T.; Loridant, S.; Volta, J.-C. *J. Phys. Chem. B* **2003**, *107*, 11475.
(23) Laberty-Robert, C.; Long, J. W.; Lucas, E. M.; Pettigrew, K. A.; Stroud, R. M.; Doescher, M. S.; Rolison, D. R. *Chem. Mater.* **2006**, *18*, 50.
(24) Trovarelli, A.; de Leitenburg, C.; Boaro, M.; Dolcetti, G. *Catal. Today* **1999**, *50*, 353.
(25) Zhu, T.; Kundakovic, L. J.; Dreher, A.; Flytzani-Stephanopoulos, M. *Catal. Today* **1999**, *50*, 381.
(26) Solinas,V.; Rombi, E.; Ferino I.; Cutrufello, M. G.; Colón, G.; Navío, J. A. *J. Mol. Catal. A: Chem.* **2003**, *204−205*, 629.
(27) Appel, L. G.; Eon, J. G.; Schmal, M. *Phys. Status Solidi* **1997**, *163*, 107.
(28) Kašpar, J.; Fornasiero Graziani, M. *Catal. Today* **1999**, *50*, 285.

10.1021/cm062912r CCC: $37.00
Published on Web 05/19/2007

hydrocarbons,[16,19,24,28] wet oxidation processes of organic compounds,[16,30,31] the removal of total organic carbon from industrial wastewaters,[30,31] the automotive exhaust gas conversion,[17,18,24] water-gas shift reaction,[32−34] methane reforming with CO_2,[20,35−38] SO_2 reduction with CO,[25] and finally, in deNOx catalysis.[39−42] To summarize this overview of its applicability: there is no doubt that, in industrial catalysis, CeO_2 is the most significant among the oxides of rare earth elements.

However, it is well-known that the catalytic activity of pure ceria may be affected by some of its innate properties. The catalytic efficiency of ceria may be reduced at elevated temperatures because of sintering and loss of surface area;[43] sintering also causes a loss of oxygen storage capacity. Besides, the preparation of ceria-containing materials with sufficiently high specific surface area is still not well-known technology. Therefore, attempts to amplify the desired properties of ceria have been made: although its electrical properties can be adjusted by doping with heterovalent cations;[5,6,9,13] in the domain of catalysis, the formulations where ceria is spread over a thermally stable, high-surface-area support or thoroughly mixed with other oxides have been synthesized and investigated. Ceria stabilized on alumina or silica[16,18,27,44−48] has been found to be an efficient catalyst, especially for environmental applications such as combustion or removal of pollutants from auto-exhaust streams. For the same reasons, special attention has been focused recently on the preparation of ceria−zirconia solid solutions.[17,18,22,26,49] Despite the fact that ceria-based mixed-oxide systems have been widely investigated, there is still big interest in adjusting their properties that are important for catalytic applications.

In this work, we investigated mixed-oxide formulations including CeO_2, which could have applications in the domain of environmentally important processes. It is known that india and gallia are good catalysts in NO_x removal and in oxidation reactions such as combustion of methane traces.[17,50−53] Therefore, the present work focuses on the combination of ceria with another oxide from group III (boria, alumina, gallia and india) in order to investigate the possibility of optimizing the surface properties of thus obtained mixed oxides, important for their catalytic behavior in depollution processes.

After searching the relevant scientific literature, it draws attention to the completely different preparation protocols that are used to obtain ceria-based mixed-oxide systems. The preparation method is crucial for all important characteristics of one "green" catalyst. The examples of different catalytic activities have been shown in the literature for the same mixed-oxide formulations but prepared by coprecipitation and sol−gel routes.[54] Among the other known techniques, such as hydrothermal and surfactant-templated synthesis,[55] sol−gel[23] and mimic methods,[56] ultrasound irradiation, etc.,[57] coprecipitation is still the most straightforward method known to provide good dispersion and homogeneous distribution of mixed metal oxides in bulk.[25,54,57−59] Therefore, in this investigation, the desired materials, $B_2O_3-CeO_2$, $Al_2O_3-CeO_2$, $Ga_2O_3-CeO_2$, and $In_2O_3-CeO_2$, were synthesized using the coprecipitation method. Having in mind the importance of all surface properties for catalytic behavior, we fully characterized the synthesized mixed-oxide samples with respect to their structural, textural, acid−base, and red−ox features.

2. Experimental Section

2.1. Sample Preparation. In this work, cerium mixed oxides with a range of Me_2O_3 (Me: B, Al, Ga, In) contents were prepared, in order to investigate both the influence of Me_2O_3 character and its content on all investigated characteristics. The compounds used as Me_2O_3 precursors used along the synthesis by coprecipitation were boric acid (H_3BO_3, Merck) and the nitrates of aluminum, gallium, and indium: $Al(NO_3)_3 \cdot 9H_2O$ (≥99%, Fluka), $Ga(NO_3)_3 \cdot 5H_2O$ (99.9% Alfa Aesar), and $In(NO_3)_3 \cdot 5H_2O$ (99.9%, Aldrich). The precursor for the ceria phase was cerium(IV) ammonium nitrate ($(NH_4)_2Ce(NO_3)_6$, 99+% Alfa Aesar). The requested quantities of the group III metal oxide and ceria precursor were dissolved in deionized water at room temperature; the exception was H_3BO_3, for which 50 °C was chosen as the optimum temperature for dissolving, in order to increase its solubility and prevent its

(29) Garcia, T.; Solsona, B.; Taylor, S. H. *Catal. Lett.* **2005**, *105*, 183.
(30) Imamura, S.; Fukuda, I.; Ishida, S. *Ind. Eng. Chem. Res.* **1988**, *27*, 718.
(31) Mishra, V. S.; Mahajani, V. V.; Joshi, J. B. *Ind. Eng. Chem. Res.* **1995**, *34*, 2.
(32) Weibel, M.; Garin, F.; Bernhardt, P.; Maire, G.; Prigent, M. *Stud. Surf. Sci. Catal.* **1991**, *71*, 195.
(33) Zafiris, G. S.; Gorte, R. J. *J. Catal.* **1993**, *139*, 561.
(34) Jacobs, G.; Khalid, S.; Patterson, P. M.; Sparks, D. E.; Davis, B. H. *Appl. Catal., A* **2004**, *268*, 255.
(35) Trovarelli, A. *Catal. Rev.−Sci. Eng.* **1996**, *48*, 439.
(36) Montoya, J. A.; Romero-Pascual, E.; Gimon, C.; Del Angel, P.; Monzon, A. *Catal. Today* **2000**, *63*, 71.
(37) Craciun, R.; Daniell, W.; Knözinger, H. *Appl. Catal., A* **2002**, *230*, 153.
(38) Asami, K.; Li, X.; Fujimoto, K.; Koyama, Y.; Sakurama, A.; Kometani, N.; Yonezawa, Y. *Catal. Today* **2003**, *84*, 27.
(39) Kawi, S.; Tang, Y. P.; Hidajat, K.; Yu, L. E. *J. Metastable Nanocryst. Mater.* **2005**, *23*, 95.
(40) Neylon, M. K.; Castagnola, M. J.; Castagnola, N. B.; Marshall, Ch.L. *Catal. Today* **2004**, *96*, 53.
(41) Baudin, F.; Da Costa, P.; Thomas, C.; Calvo, S.; Lendresse, Y.; Schneider, S.; Delacroix, F.; Plassat, G.; Djega-Mariadassou, G. *Top. Catal.* **2004**, *30/31*, 97.
(42) Kašpar, J.; Fornasiero, P. *J. Solid State Chem.* **2003**, *171*, 19.
(43) Schmieg, S. J.; Belton, D. N. *Appl. Catal., B* **1995**, *6*, 127.
(44) Piras, A.; Trovarelli, A.; Dolcetti, G. *Appl. Catal., B* **2000**, *28*, L77.
(45) Djuričić, B.; Pickering, C. S.; McGarry, D.; Tambuyser, P.; Thomas, P. *J. Mater. Sci.* **1999**, *34*, 1911.
(46) Fullerton, D. J.; Westwood, A. V. K.; Brydson, R.; Twigg, M. V.; Jones, J. M. *Cat. Today* **2003**, *81*, 659.
(47) Damyanova, S.; Perez, C. A.; Schmal, M.; Bueno, J. M. C. *Appl. Catal., A* **2002**, *234*, 271.
(48) Craciun, R. *Solid State Ionics* **1998**, *110*, 83.
(49) Reddy, B. M.; Khan, A.; Yamada, Y.; Kobayashi, T.; Loridant, S.; Volta, J.-C. *Langmuir* **2003**, *19*, 3025.
(50) Perdigon-Melon, J. A.; Gervasini, A.; Auroux, A. *J. Catal.* **2005**, *234*, 421.
(51) Gervasini, A.; Perdigon-Melon, J. A.; Guimon, C.; Auroux, A. *J. Phys. Chem. B* **2006**, *110*, 240.
(52) Park, P. W.; Ragle, C. S.; Boyer, C. L.; Lou Balmer, M.; Engelhard, M.; McCready, D. *J. Catal.* **2002**, *210*, 97.
(53) Zahir, Md. H.; Katayama, S.; Awano, M. *Mater. Chem. Phys.* **2004**, *86*, 99.
(54) Pintar, A.; Batista, J.; Hočevar, S. *J. Colloid Interface Sci.* **2005**, *285*, 218.
(55) Cracium, R.; Daniell, W.; Knozinger, H. *Appl. Catal., A* **2002**, *230*, 153.
(56) Li, J. G.; Ikegami, T.; Lee, J. H. *Acta Mater.* **2001**, *49*, 419.
(57) Yu, J. C.; Zhang, L.; Lin, J. *J. Colloid Interface Sci.* **2003**, *260*, 240.
(58) Lee, J.-S.; Choi, K.-H.; Ryu, B.-K.; Shin, B-C.; Kim, I.-S. *Mater. Res. Bull.* **2004**, *39*, 2025.
(59) Letichevsky, S.; Tellez, A.; de Avillez, R. R.; da Silva, M. I. P.; Fraga, M. A.; Appel, L. G. *Appl. Catal., B* **2005**, *58*, 203.

Table 1. Chemical Analysis and BET Surface Areas of Investigated Samples

sample	label	ICP/Me^{3+} (wt %)	ICP/ Me_2O_3 (wt %)	atomic ratio Me/Ce, XPS (surface)	BET surface area ($m^2\ g^{-1}$)
	BCe-6	2.0	6.4	0.50	92
	BCe-8	2.5	8.1	0.60	92
$B_2O_3-CeO_2$	BCe-17	5.4	17.4	1.60	95
	AlCe-8	4.1	7.8	0.40	152
$Al_2O_3-CeO_2$	AlCe-22	11.4	21.6	1.70	219
	GaCe-6	4.5	6.1	1.50	142
$Ga_2O_3-CeO_2$	GaCe-16	11.5	15.5	1.90	117
	InCe-6	4.6	5.6	0.10	125
	InCe-8	6.7	8.1	0.15	93
$In_2O_3-CeO_2$	InCe-14	11.9	14.4	0.50	134
CeO_2	CeO_2				88

evaporation/decomposition, in the same time. The solutions were mixed with a continuous monitoring of pH. Dilute ammonia (28% wt/wt) was added gradually dropwise to this mixture of two solutions with vigorous stirring, until the precipitation was complete (pH 8). Pure ceria was obtained by precipitation from a solution of $(NH_4)_2Ce(NO_3)_6$ by ammonia in the same way. All precipitates were filtrated and washed with hot distilled water (0.5 L). Subsequently, the precipitated materials were flushed twice in absolute ethanol solution in order to facilitate agglomeration, dried overnight in an oven at 110−120 °C and calcined in air at 500 °C for 5 h; the temperature applied for calcination has been chosen on the basis of TG measurements.

The samples investigated in this work are denoted as XCe-*n*, where X denotes B, Al, Ga, or In, whereas *n* is the number presenting the weight percent of group III metal oxide in the respective sample. The list of prepared catalysts and their labels are summarized in Table 1.

2.2. Characterization. The prepared materials were fully characterized. Chemical compositions (the contents of metals and metal oxides) were determined by AES-ICP in a Spectroflame-ICP instrument, after the samples were dissolved using the mixture of inorganic acids (H_2SO_4 and HNO_3).

After the preparation, crude samples were calcined, with the intention of decomposing the nitrates and removing the water and impurities from their bulk. To determine the appropriate (the lowest) temperature needed for calcinations of fresh samples, thermogravimetry (TG-dTG) was applied. TG-dTG measurements were performed on a "Labsys−TG" Setaram equipment. The crude samples (∼50 mg) were heated from 25 to 500 °C with a heating rate of 5 °C min^{-1} in a flow of air, which was chosen as a soft oxidizing agent for calcinations.

The structural, textural, and surface properties of calcined samples were investigated using different techniques: low-temperature nitrogen adsorption, powder X-ray diffraction (XRD), Raman spectroscopy, scanning electron microscopy (SEM), and X-ray photoelectron spectroscopy (XPS).

The adsorption of nitrogen was performed at −196 °C, after pretreatment performed for 4.0 h at 400 °C under a vacuum; surface areas were determined by the BET method from the resulting isotherms.

The crystalline structure was examined using XRD and Raman techniques. XRD patterns were recorded on a Bruker (Siemens) D5005 diffractometer at room temperature using Cu Kα radiation (0.154 nm) from 3 to 80° in a 0.02° steps with 1 s per step. The Raman spectra of investigated samples were collected on a DILOR XY spectrometer, equipped with a liquid-nitrogen cooled charge-coupled device (CCD) detector. The excitation was provided by the 514.5 nm line of an Ar^+ Kr^+ ion laser (Spectra Physics), keeping the sample under a microscope, under the ambient atmosphere. The power of the incident beam on the sample was 3 mW. Because the laser beam can be precisely focused, it was possible to perform quantitative evaluation of band intensities between samples studied.[60] The width of the analyzed spot for each sample was ∼1 μm. The time of acquisition was adjusted according to the intensity of the Raman scattering. The wavenumber values reported from the spectra are accurate to within 2 cm^{-1}. For each solid, the spectra were recorded at several points of the sample (more than six) to ascertain the homogeneity of the sample; the average of all these spectra were plotted and presented in this paper.

The morphologies of the samples have been examined using SEM; the images were obtained using a Jeol 55 CF microscope (CMEABG Lyon).

The analysis of elemental surface concentrations was performed by means of XPS technique, which was done using a SSI (Surface Science Instruments) 301 spectrophotometer with a monochromatic Al Kα radiation source, equipment that is fully described elsewhere.[61] The XPS analysis depth was around 5−10 nm. The XP spectra of Al (2p), O (1s), Ce ($3d_{5/2}$), B (1s), Ga ($2p_{3/2}$), and In ($3d_{5/2}$) were recorded in detail. The binding energy of the $Ce3d^{5/2}$ line (CeO_2), chosen as internal reference, is 882.2 eV for all samples.

The redox properties of the investigated samples have been studied by temperature-programmed reduction−temperature-programmed oxidation (TPR−TPO) experiments. The experimental setup, the quantification of the signal, and the acquisition of the data for these measurements have been described in detail elsewhere.[62] Briefly, the system is equipped with a TCD (thermal conductivity detector), which produces an output signal that is proportional to the concentration of hydrogen or oxygen in the carrier gas. The sample was held on the frit of a U-shape quartz reactor, allowing the reducing or oxidizing gas stream to pass through the sample. The catalyst samples used weighed about 0.1500 g. Prior to the TPR experiment, the sample was heated to 400 °C in an argon flow and kept at the same temperature for 3 h; subsequently, it was cooled down to room temperature. TPR was performed in situ up to 830 °C in a H_2 flow (5%/Ar). After cooling down to room temperature, the sample was flushed overnight with helium. TPO was performed up to 830 °C in a flow of oxygen (1%/He). The flow rate of all gases was 20 mL min^{-1}, and the heating rate for all ramps during experiment was 5 °C min^{-1}. For InCe-14, TPR−TPO experiments were additionally performed up to 500 °C.

The acid−base properties were studied using the adsorption of probe molecules (NH_3 and SO_2) by means of two appropriate methods: adsorption microcalorimetry and XPS. Microcalorimetric

(60) Skoog, A.; Leary, J. *Principles of Instrumental Analysis: 13Raman Spectroscopy*, 4th ed.; Harcourt Brace College Publishers, Orlando, FL, 1992; p 302.
(61) Keranen, J.; Guimon, C.; Iiskola, E.; Auroux, A.; Niinisto, L. *J. Phys. Chem. B* **2003**, *107*, 10773.
(62) Jouguet, B.; Gervasini, A.; Auroux, A. *Chem. Eng. Technol.* **1995**, *18*, 243.

studies were performed at 80 °C in a heat flow calorimeter (C80 from Setaram) linked to a conventional volumetric apparatus equipped with a Barocel capacitance manometer for pressure measurements. The samples were pretreated in a quartz cell by heating overnight under a vacuum at 400 °C with a heating rate of 0.6 °C min^{-1}. The differential heats of adsorption were measured as a function of coverage by repeatedly sending small doses of respective gas onto the sample until an equilibrium pressure of about 67 Pa was reached. The sample was then outgassed for 30 min at the same temperature, and a second adsorption run was performed at 80 °C on each sample, until an equilibrium pressure of about 27 Pa was attained. The difference between the amounts adsorbed in the first and second adsorptions at 27 Pa represents the irreversibly chemisorbed amount (V_{irr}) of a respective gas, which provides the estimation of the number of strong acidic/basic sites.

For the investigation of NH_3 or SO_2 adsorptions by XPS, the samples were activated overnight under helium at 350 °C and subsequently exposed to one of the probes, at 80 °C. The adsorption was followed by desorption for 1 h under helium at the same temperature. The XPS measurements were performed at room temperature, preserving inert conditions during all sample handling steps (with the help of a glove box coupled with the introduction chamber of the spectrometer). NH_3 or SO_2 adsorptions were investigated through the recording of N1s or S2p lines, respectively.

3. Results and Discussion

3.1. Chemical Composition, Structure and Morphology of the Samples. Table 1 presents the list of the samples synthesized in this work, their chemical compositions, obtained by ICP, surface concentrations obtained by XPS technique, and the values of BET surface areas.

It is widely accepted that for most catalytic applications, solid materials with high specific surface areas are desirable. Experience has shown that in general, low-temperature pretreatment processes are necessary to obtain oxides with high surface areas, poor crystallinity, and small particle sizes.[63] As it is well-known that the temperature of calcination can influence the morphology of a final product, it was important to determine the lowest temperature, which is high enough to achieve the complete decomposition of nitrates, the removal of water, and impurities from the bulk of a sample. In this work, thermogravimetric analysis was performed in order to determine this minimal temperature needed for calcination of the crude sample.

Figure 1 presents the TG and dTG profiles obtained for InCe-14 uncalcined sample. Three well-resolved peaks are found in dTG, thus indicating the existence of three separated desorption processes. The low-temperature process exhibits a peak with a maximum centered between 80 and 100 °C; it is finished up to 150 °C and originates from the loss of molecularly adsorbed water from the surface. The second process has a maximum in the temperature range from 230 to 250 °C and can be attributed to the decomposition of nitrates and the major loss of the impurities and water from the bulk. The third peak ($T_{max} \approx 440$ °C) corresponds to the lowest mass loss, and according to the literature, it can be attributed to the dehydroxylation of surface and loss of impurities such as the remaining nitrates and carbonate ions.

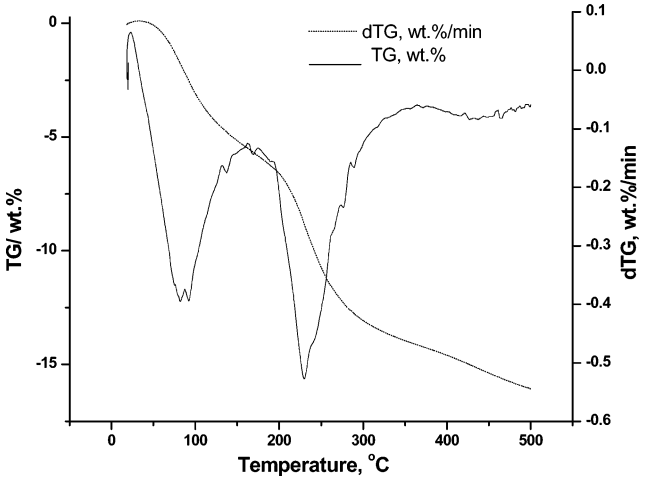

Figure 1. TG-dTG profiles obtained for uncalcined InCe-14.

The mass losses vary according to the type of group III metal oxide mixed with ceria. Thermograms obtained for the samples with similar amounts of Me_2O_3 show that the majority of mass losses found in TG-dTG experiments originates from the removal of molecular/physisorbed water with the masses evolved from the samples ordered as follows: AlCe-22 > InCe-14 > GaCe-16. This result correlates well with the known fact that alumina expresses higher hydrophilic character in comparison with gallia, for example.[64] However, the results of TG-dTG experiments have shown that mass decreases of about 2−7% were still observed in the temperature region from 450 up to 500 °C. On the basis of these data, 500 °C was chosen for the calcination of the samples prepared in this work.

BET surface areas of calcined samples are given in Table 1. Importantly, higher surface areas were observed for mixed oxides in comparison with that of pure ceria (88 m^2 g^{-1}). This increasing BET surface areas could be explained by high dispersion of two oxides that happens as a result of mixed oxides forming by the coprecipitation method, as can be seen from a SEM micrograph obtained for the InCe-14 sample and presented in Figure 2. High uniformity explains the higher BET surface area found for this sample, in comparison with pure ceria.

The insight into the data shown in column 6 (Table 1) reveals the evidence that BET surface areas are dependent on the type of group III metal oxide: the highest surface areas were obtained for alumina-containing samples. Besides, BET surface areas are evidently dependent on the amount of group III metal oxide.

The powder XRD patterns of various mixed oxides investigated in this work were recorded under ambient conditions. In accordance with the data that have been already reported in the literature for the case of ceria mixed with silica, titania, or zirconia,[22] the XRD patterns showed only the diffractions of fluorite structure of CeO_2. Besides, poor cristallinity is a characteristic of all mixed oxides investigated here, only the broad diffraction lines due to CeO_2 could be observed. Importantly, the intensities of XR diffraction lines specific to CeO_2 are lower in comparison

(63) Kung, H. H. *Studies in Surface Science Catalysis: Transition Metal Oxides: Surface Chemistry and Catalysis*; Elsevier: Amsterdam, 1989; Vol. 45, p 121.

(64) Gu, X.; Ge, J.; Zhang, H.; Auroux, A.; Shen, J. *Thermochim. Acta* **2006**, *451*, 84.

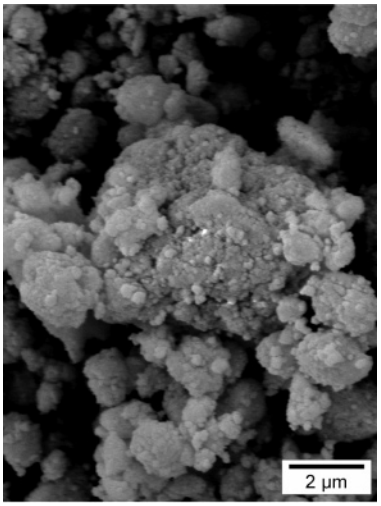

Figure 2. SEM image of InCe-14 calcined in air at 500 °C.

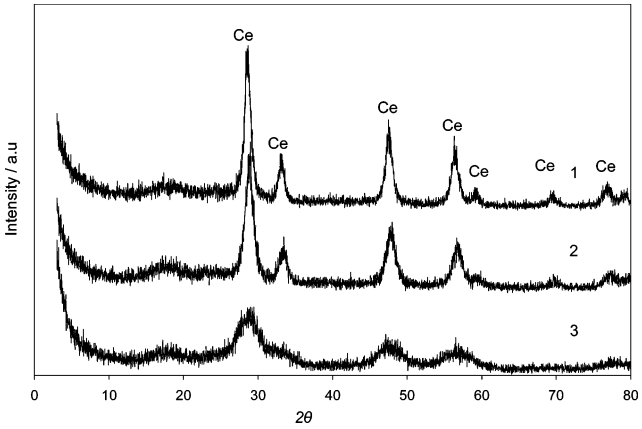

Figure 3. XRD patterns of CeO_2 and $Al_2O_3-CeO_2$ samples collected after preparation and calcination at 500 °C: (1) CeO_2, (2) AlCe-8, (3) AlCe-22.

with those found for pure ceria. As a typical example, Figure 2 gives powder XRD patterns collected for pure CeO_2 samples and two $Al_2O_3-CeO_2$ samples.

Presented diffractograms clearly show also that the decrease in X-ray diffraction intensities is related to alumina content. It also has to be mentioned from XRD measurements that there are no extra lines due to compounds or mixed phases between ceria and group III metal oxides.

Raman spectra monitored for pure CeO_2 and the samples containing the highest amounts of Me_2O_3 in mixed $Me_2O_3-CeO_2$ are presented in Figure 4. All spectra exhibit main peaks at 270, 464, and 600 cm^{-1} that have already been assigned to the CeO_2 phase.[22] In consistence with XRD measurements, Raman lines that could be assigned to Me_2O_3 were not observed. However, it is important to notice that the main peak assigned to ceria (at 464 cm^{-1}) was shifted to lower wavenumbers (457 cm^{-1}) with the adding of the amount of second metal oxides. As has been stated already, XRD measurements did not show any evidence of third compounds forming. Therefore, this shift in position of the main peak assigned to ceria in Raman spectra, noticed for mixed oxides investigated in this work, is important and indicates that some interaction between oxides happened. In addition, the decrease in intensity of the same peak was observed, as a result of mixing with the group III metal oxides. Importantly, even in the case of very close amounts

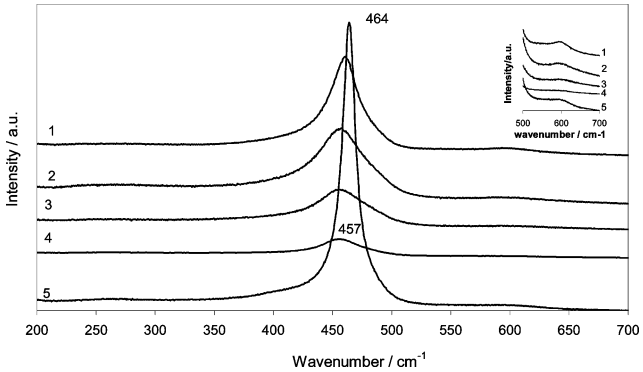

Figure 4. Raman spectra of coprecipitated samples: (1) InCe-14, (2) GaCe-16, (3) AlCe-22, (4) BCe-17, (5) CeO_2. Inset: the band centered at 600 cm^{-1}.

of Me_2O_3 mixed with CeO_2, the influence of oxide nature on the intensity of this band is evident. The following order in this intensity decrease of the peak centered at 464 cm^{-1} was found for the presented spectra: CeO_2 > InCe-14 > GaCe-16 > AlCe-22 > BCe-17. Again, these orders are in agreement with XRD data, where the same sequence in decreasing of the crystallinities can be seen with doping of the second metal.

It is known from the literature that a band recorded at 600 cm^{-1} is associated with oxygen vacancies in the CeO_{2-x} lattice,[22] and that these sites could be active in combustion reactions. Therefore, it is important to notice that this band became more pronounced for gallia−ceria and india−ceria, as presented by the inset in Figure 4. These results indicate a larger influence of gallia or india cations on CeO_2 lattice, in comparison with boria and alumina.

3.2. Acid/Base Properties. The adsorption of probe molecules (NH_3 and SO_2) was used to investigate the acid−base properties by XPS and calorimetric method. The information obtained from these investigations can be considered to supplement each other, rather than as a basis for comparison of results, because the principles of these two experimental techniques are not the same. Calorimetric study allows precise information on the concentrations of active sites (basic or acidic) on catalytic surface, whereas XPS measurements can help to differentiate the types of these sites (Brönsted or Lewis). In addition, XPS measurements of probe molecule adsorption provide information only on the strong and medium strength acid sites and do not titrate the weak sites, which cannot keep ammonia (or SO_2) molecules under ultrahigh (1×10^{-7} Pa) vacuum conditions of the analyses.

Analysis of B 1s, Al 2p, In $3d_{5/2}$, and Ce $3d_{5/2}$ XPS Bands. XPS data obtained for solid materials are summarized in Tables 2−5, which present the data for $B_2O_3-CeO_2$, $Al_2O_3-CeO_2$, $Ga_2O_3-CeO_2$ and $In_2O_3-CeO_2$ samples, respectively. The Me/Ce atomic ratio obtained by XPS (Me/Ce surface) and by ICP (Me/Ce bulk) methods are already given in Table 1. B/Ce, Al/Ce, Ga/Ce, and In/Ce ratios on the surface were determined from the XPS band areas of B 1s (Al2p, Ga2p or $In3d_{5/2}$) and $Ce3d_{5/2}$ peaks. Because of the large uncertainty on the XPS atomic percentage due particularly to the Scofield intensity factors, which are average values, only the relative atomic ratios in each series

Table 2. XPS Data for B_2O_3−CeO_2 Samples

	BCe-6		BCe-8		BCe-17		CeO_2	
adsorption (80 °C)	NH_3	SO_2	NH_3	SO_2	NH_3	SO_2	NH_3	SO_2
B/Ce	0.4	0.5	0.9	0.6	1.4	1.6		
N/(B+Ce)	0.011				0.016		0.008	
S/(B+Ce)		0.15		0.16		0.05		0.44
N1s Lewis	399.8				400.2		399.7	
L (O^{2-})		167.2		166.9		166.6		166.9
S2p$_{3/2}$		(35%)		(25%)		(15%)		(10%)
B (OH^-)		169.2		168.1		168.3		168.3
		(65%)		(75%)		(85%)		(90%)

Table 3. XPS Data for Al_2O_3−CeO_2 Samples

	AlCe-8		AlCe-22		CeO_2	
adsorption (80 °C)	NH_3	SO_2	NH_3	SO_2	NH_3	SO_2
Al/Ce	0.3	0.4	1.6	1.7		
N/(Al +Ce)	0.005		0.006		0.008	
S/(Al+Ce)		0.52		0.27		0.44
N1s Lewis	399.5		399.7		399.7	
L (O^{2-})		166.5				166.9
S2p$_{3/2}$		(15%)				(10%)
B (OH^-)		168.2		168.4		168.3
		(85%)		(100%)		(90%)

Table 4. XPS Data for Ga_2O_3−CeO_2 Samples

	GaCe-6		GaCe-16		CeO_2	
adsorption (80 °C)	[a]	SO_2	[a]	SO_2	NH_3	SO_2
Ga/Ce	1.6[b]	1.5[b]	1.8[b]	1.9[b]		
N/(Ga+Ce)					0.008	
S/(Ga+Ce)		0.36[b]		0.20[b]		0.44
N1s (Lewis)					399.7	
L (O^{2-})		167.2		167.4		166.9
S2p$_{3/2}$		(30%)		(35%)		(10%)
B (OH^-)		168.3		169.1		168.3
		(70%)		(65%)		(90%)

[a] No detected adsorption of NH_3 because of the band N1s is hidden by the $M_2L_{4,5}$ $L_{4,5}$ Auger band of Ga. [b] The quantitative data and the binding energy of the Ga3p band are approximate because of the overlap of this peak and the Ce4d band.

are considered. The quantitative data for gallia−ceria samples are approximate because of the overlapping of Ga3p and the Ce4d bands.

The XPS spectra of Ce3d core electron levels for InCe-8 and InCe-14 samples are given in Figure 5. There are six peaks corresponding to the three pairs of spin−orbit doublets of oxidized CeO_2[16] and four peaks corresponding to the two doublets of oxidized Ce_2O_3. For each doublet, $3d_{5/2}$ corresponds to the label v and $3d_{3/2}$ to u. Explanation of the origin of each doublet is given in details in work of Reddy et al.[22] The peaks labeled v/u, v″/u″, v‴/u‴ have been assigned to Ce^{4+} and v′/u′,v_0/u_0 to Ce^{3+}. Two main bands of $Ce3d_{5/2}$[65] at 882.2 eV (v) corresponded to Ce^{4+} and 885.4 eV (v′) corresponded to Ce^{3+}; these were observed for all samples (Tables 2−5). However, XRD could not detect any visible Ce_2O_3 lines. The cerium is mainly present in the Ce^{4+} oxidation state (up to 70−80 at %). The presence of Ce(III) can be mainly attributed to removal of surface hydroxyl groups and oxygen from CeO_2 surface during exposure of the samples to the X-ray in an ultrahigh vacuum chamber (UHV) under mild reduction conditions.[47] This phenomena is confirmed by the increase in the intensity of the components corresponding to Ce(III) with the irradiation time of the sample. XPS Ce3d peaks of Ce^{4+} and Ce^{3+} of In 6.7-Ce sample are broader relative to the same peaks of InCe-14. The broader cerium band could be related to better distribution of indium oxide within the bulk sample as consequence of this better interaction with cerium oxide. The core-level spectra of B1s (191.1 eV) in the case of boria−ceria binary oxides showed a shift toward low-binding energies (BE) in comparison with pure B_2O_3 (193.5 eV),[66,67] indicating the interaction between the two oxides. The changes of BE of Al2p,[68] 74.2 ± 0.8 eV, and In $3d_{2/5}$,[68] 444.3 ± 0.3 eV, were observed as well for alumina−ceria and india−ceria.

Analysis of S 2p and N 1s XPS. XPS experiments have shown that all the samples have more basic than acidic character, as the S/(Me+Ce) molar ratios were largely greater than the corresponding N/(M+Ce). The atomic ratios of S/(Me+Ce) and N/(Me + Ce) were measured from the ratio between the intensity of the main band associated with the adsorbed sulfide or ammonia molecules (where S is S2p band for SO_2, and N is N1s for NH_3) and the bands associated with metal oxide (where Me is Al2p for Al_2O_3 , B1s for B_2O_3 , Ga3p for Ga_2O_3, $In3d_{5/2}$ for In_2O_3 and $Ce3d_{5/2}$ for CeO_2). The quantitative data and the binding energy of the Ga3p band are particularly approximate because of the overlap of this peak and the Ce4d band. It is the same for the quantitative results (N/Ga+Ce) after adsorption of ammonia because of the overlap between the band N1s of nitrogen and the Auger band $L_2M_{45}M_{45}$ of gallium. In all cases, the quantitative analysis of NH_3 adsorption is difficult because of the very weak concentration of adsorbed ammonia and thus the large signal-to-noise ratio. This can come from a small concentration of surface acidic sites or from a weak strength of these sites (provoking a partial desorption of NH_3 in the UHV conditions of the XPS analyses). The obtained results are in the range 1×10^{-2} to 1×10^{-3} at % (Figure 6). It seems that boria−ceria samples exhibit higher acidic character, which is in agreement with the calorimetric measurements. XPS spectra of mixed samples showed N1s bands of BE in the range 399.0−400.2 eV that are assigned to ammonia adsorption on Lewis acid sites.[69]

The values of binding energies and the percent proportions of the sulfur species adsorbed on Lewis basic sites (SO_2−O^{2-}) or Brönsted basic sites (SO_2−OH^-) are summarized

(65) Galtayries, A.; Sporken, R.; Riga, J.; Blanchard, G.; Caudano, R. *J. Electron Spectrosc. Relat. Phenom.* **1998**, *88*−*91*, 951.

(66) Rivière, J. P.; Cahoreau, M.; Pacaud, Y. *Thin Solid Films* **1993**, *227*, 4.

(67) Nefedov, V. I.; Gati, D.; Dzhuinskii, B. F.; Sergushin, N. P.; Salyn, Y A. V. *Z. Neorg. Khim.* **1975**, *20*, 2307.

(68) Wagner, C. D.; Riggs, W. M.; Davis, L. E.; Moulder, J. F.; Muilenberg, G. E. *Handbook of X-ray photoelectron spectroscopy*. Perkin-Elmer Corporation, Physical Electronics Division: Eden Prairie, MN, 1979; p 116.

(69) Guimon, C.; Gervasini, A.; Auroux, A. *J. Phys. Chem. B* **2001**, *105*, 10316.

Table 5. XPS Data for $In_2O_3-CeO_2$ Samples

	InCe-6		InCe-8		InCe-14		CeO_2	
adsorption (80 °C)	NH_3	SO_2	NH_3	SO_2	NH_3	SO_2	NH_3	SO_2
In/Ce	0.09	0.10	0.15	0.15	0.5	0.5		
N/(In+Ce)	0.004		0.008		0.003		0.008	
S/(In+Ce)		0.38		0.66		0.30		0.44
N1s Lewis	399.5		399.4		399		399.7	
L (O^{2-})		167.1		166.7		166.6		166.9
S2p$_{3/2}$		(10%)		(25%)		(15%)		(10%)
B (OH^-)		168.5		168.5		168.1		168.3
		(90%)		(75%)		(85%)		(90%)

in Tables 2−5. Figure 7 presents an example of XPS S2p peak obtained after adsorption of SO_2 at 80 °C on the investigated mixed oxides. This peak is decomposed into two doublets ($2p_{3/2}-2p_{1/2}$) regardless of the sample composition. The first $2p_{3/2}$ peak appeared at about 167 eV and the second peak appeared at 169 eV. As in the case of TiO_2,[69] the former doublet could be assigned to SO_2 in interaction with O^{2-} anions, i.e., to Lewis basic sites. The latter doublet could correspond to the interaction of SO_2 molecules with hydroxyl (OH^-) surface groups (Brönsted sites). This assignment is proposed on the basis of the evolution of the relative intensities of the components according to the activation temperature (Figure 7, spectra 1 and 2). Indeed, when the activation temperature is increased from 350 to 700 °C, the relative intensity of the first doublet associated with the sulfite groups (167 eV for $S2p_{3/2}$) increases (from 10%, Figure 7 spectrum 1, to 25%, Figure 7 spectrum 2). This evolution can be related to a smaller concentration of OH^- groups after activation at high-temperature (more effective dehydroxylation of the surface at 700 °C). In the same time, the S/Ce atomic ratio decreases from 0.44 to 0.17, this is in agreement with the disappearance of an important part of the Brönsted sites, whereas the concentration of the Lewis centers remains quasiconstant. The relative ratio of B(OH^-) and L(O^-) bands shows that the main part of the surface basicity for all samples stamps from surface hydroxyl groups. The following orders in decreasing of surface basic sites concentrations can be given

- boria-containing samples: BCe-8 ≈ BCe−6 > BCe-17 (Figure 8, Table 2);
- alumina-containing samples: AlCe-8 > AlCe-22 (Table 3);
- gallia-containing samples: GaCe-6 > GaCe-16 (Table 4);
- indium-containing samples: InCe-8 > InCe-6 > InCe-14 (Table 5).

Microcalorimetric Results. Table 6 compiles the data obtained from microcalorimetric measurements of SO_2 and NH_3 adsorption on all investigated samples. The table presents the total amounts of adsorbed gases, the amounts of irreversibly adsorbed (chemisorbed), and the amounts of reversibly adsorbed (physisorbed) gases. As the investigated samples display noticeable differences in BET surface area values (see Table 1), the calorimetric results are

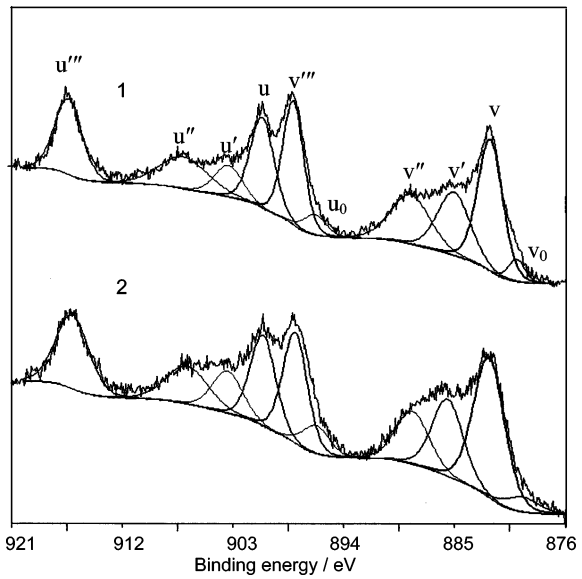

Figure 5. XPS Ce3d spectra of (1) InCe-14 with 20% Ce^{III} and (2) InCe-8 with 25% Ce^{III} after activation (He, 350 °C) and adsorption of NH_3 at 80 °C.

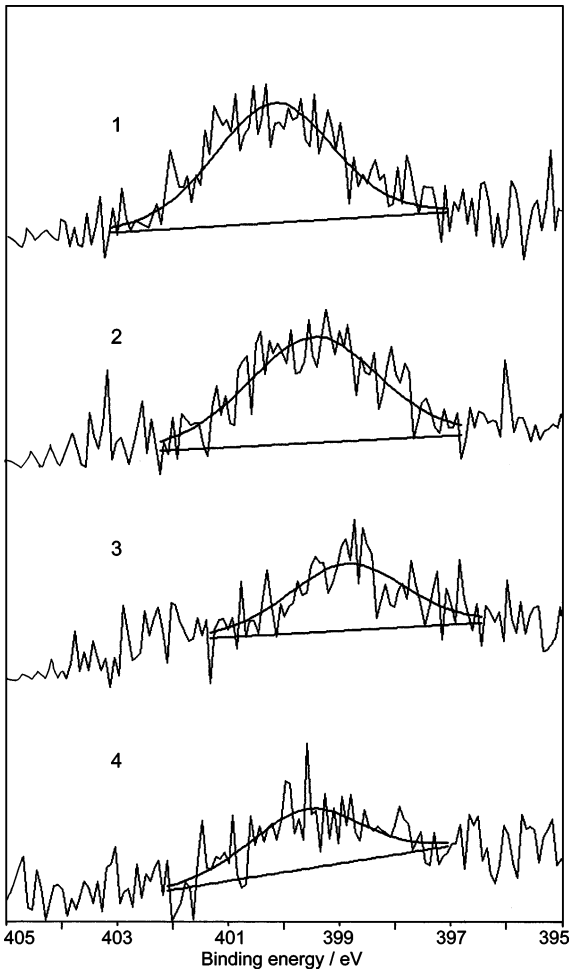

Figure 6. XPS N1s spectra of (1) BCe-17, (2) AlCe-22, (3) InCe-14, and (4) CeO_2 after activation (He, 350 °C) and adsorption of NH_3 at 80 °C.

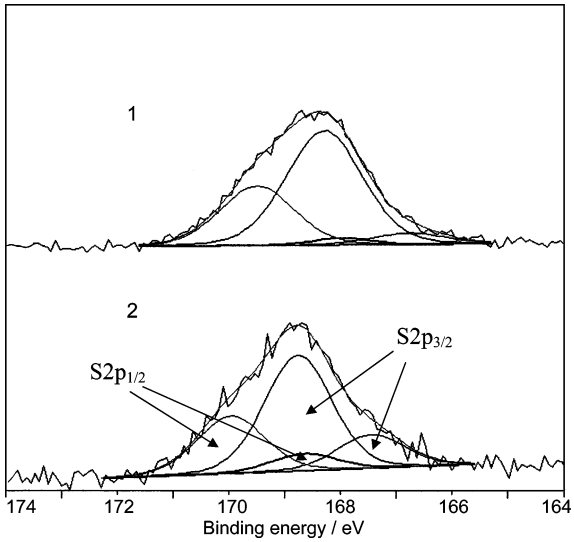

Figure 7. S2p ($2p_{3/2}-2p_{1/2}$) XPS spectra of CeO_2 activated at 350 (1) and 700 °C (2), after adsorption of SO_2 at 80 °C.

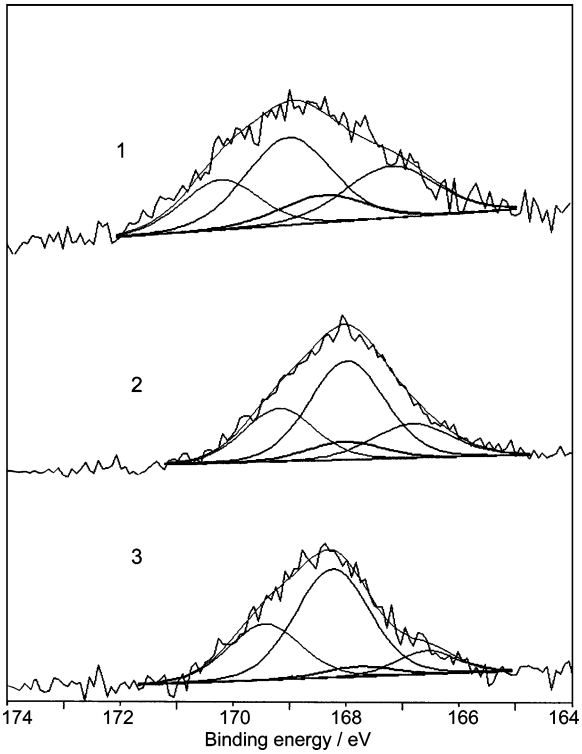

Figure 8. S2p XP spectra of (1) BCe-6, (2) BCe-8, and (3) BCe-17 activated at 350 °C, after adsorption of SO_2 at 80 °C.

presented in μmol m^{-2} rather than in μmol g^{-1}. As was already mentioned in Experimental Section, by subtracting the adsorbed volume of the secondary isotherm (not presented in the figure) from that of the primary isotherm at the same equilibrium pressure ($P = 27$ Pa), the amount of irreversibly adsorbed gas was calculated. The vertical parts of the isotherms correspond to irreversible adsorption, whereas the horizontal parts can be assigned to reversible adsorption.[70]

Figure 9 presents the isotherms obtained for SO_2 adsorption on the investigated samples. It can be concluded from

(70) Dragoi, B.; Gervasini, A.; Dumitriu, E.; Auroux, A. *Thermochim. Acta* **2004**, *420*, 127.

Table 6. Calorimetric Measurements for SO_2 and NH_3 Adsorption

	SO_2 amount adsorbed at 80 °C (μmol m^{-2})			NH_3 amount adsorbed at 80 °C (μmol m^{-2})		
sample	Nt[a]	Nread[b]	Nirr[c]	Nt	Nread	Nirr
BCe-6	1.44	0.47	0.97	2.57	1.29	1.28
BCe-8	1.10	0.32	0.78	2.53	1.20	1.33
BCe-17	0.16	0.08	0.08	3.41	1.18	2.23
AlCe-8	3.51	0.32	3.19			
AlCe-22	2.9	0.25	2.65	1.47	0.76	0.71
GaCe-6	3.97	0.48	3.49			
GaCe-16	3.73	0.44	3.29	1.91	0.95	0.95
InCe-6	3.75	0.50	3.25			
In Ce-8	3.95	0.59	3.36			
InCe-14	3.91	0.47	3.44	1.75	1.03	0.72
CeO_2	3.73	0.50	3.23	1.88	1.05	0.83

[a] Total amount of gas (μmol m^{-2}) adsorbed under an equilibrium pressure of 26.6 Pa. [b] Physisorbed amount of gas (μmol m^{-2}) determined under equilibrium pressures of 26.6 Pa by readsorption after pumping. [c] Number of the strongest sites corresponding to the irreversibly adsorbed gas amount (Nirr) calculated by subtracting the primary (Nt) and secondary (Nread) isotherms (μmol m^{-2}).

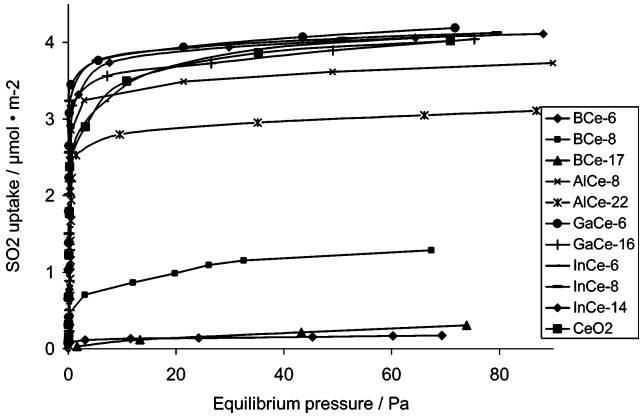

Figure 9. Isotherms obtained from SO_2 adsorption microcalorimetry experiments.

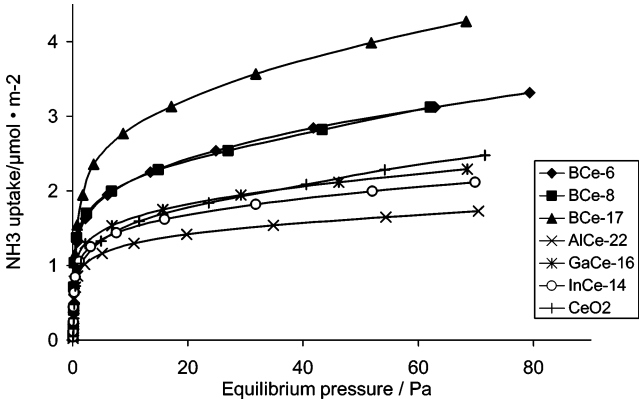

Figure 10. Isotherms obtained from NH_3 adsorption microcalorimetry experiments.

the results presented in Table 6 and in Figure 9 that the type of group III metal oxide has a decisive role for a basic character of investigated mixed oxides. The lowest adsorption of SO_2 was found for boria-containing samples; the increase of boria content produced the decrease of the amount of adsorbed gas (both total and irreversible). In the case of alumina and gallia, values comparable with those obtained for pure ceria were obtained. Only in the case of india–ceria samples were the amounts of adsorbed SO_2 slightly higher than in the case of CeO_2. However, the insight into the data presented in Table 6 gave evidence that remarkable

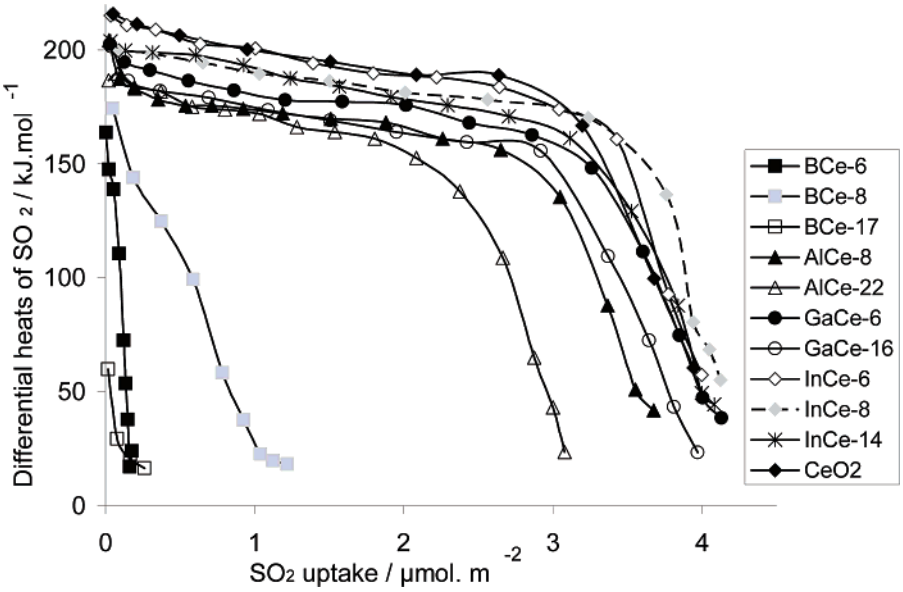

Figure 11. Differential heats of SO_2 adsorption versus coverage (SO_2 uptake in μmol m^{-2}).

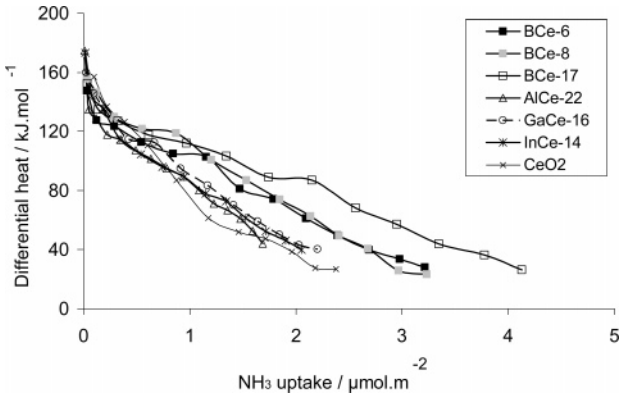

Figure 12. Differential heats of NH_3 adsorption versus coverage (NH_3 uptake in μmol m^{-2}).

differences in uptakes of SO_2 can be also noticed for different loadings of Me_2O_3.

The volumetric data obtained for NH_3 adsorption are also summarized in Table 6, whereas the isotherms of ammonia adsorption are shown in Figure 10. It is evident that only boria created significant acidity. Increasing the loading of boria in boria−ceria samples increases the number of acid sites, which can be clearly recognized through the increase of total and irreversibly adsorbed amounts of ammonia. Let us recall here that XPS spectra of ammonia adsorption showed only the presence of Lewis acid sites on catalytic surface.

Figure 11 displays the differential heats of SO_2 adsorption on the investigated mixed oxides, whereas Figure 12 presents the results of differential heats of ammonia adsorption. The profiles: differential heats vs uptake of the probe gas are multi-indicative; they give the data concerning the amount, strength, and distribution of the active sites. Besides, the values of initial heats of adsorption characterize the strongest sites active in adsorption process.

Ceria investigated in this work exhibited strong basicity: the initial heats of SO_2 adsorption are very high, above 200 kJ mol^{-1}. The addition of group III metal oxide changed the basicity of ceria. The addition of small amounts of india did not produce significant changes in the profile of differential heats; however, with increasing In_2O_3 content, the basicity of india−ceria decreased visibly; similar behavior has been observed for gallia−ceria catalysts. A more pronounced decrease in basicity has been observed for alumina−ceria materials.

In accordance with the results presented previously, the addition of small amounts of acidic boria drastically changes the profiles of differential heat of SO_2 adsorption; sharp decreasing profiles, dependent on the amount of added boria, have been found for differential heats of SO_2 adsorption.

The profiles of differential heats of ammonia adsorption vs gas uptakes presented in Figure 12 confirm previously observed acid/basic characteristics of investigated materials: although all investigated samples exhibited high initial differential heats for ammonia adsorption ($\geq$150 kJ mol^{-1}), continuous decreasing of differential heats of NH_3 adsorption were found. The profiles indicate the lowest acidity of alumina−ceria and the highest one for the case of boria−ceria samples.

Generally, it can be stated that, in comparison with pure ceria, the basicity decreased for boria−ceria samples (sharply), which is coherent with the XPS data, and for alumina−ceria samples (slightly), whereas it is similar or slightly increased for gallia−ceria and india−ceria samples. Evidently, the additions of gallium and indium oxides create some additional basic sites on ceria surface, which can be inferred from the amounts of irreversibly adsorbed SO_2 (see Table 6). These results are also in good agreement with the S/Ce ratios given by XPS.

3.3. Red−Ox Properties. Among the investigated Me_2O_3, only indium oxide can be completely reduced at relatively low temperature; therefore, this investigation was focused on reduction/oxidation of india containing samples. It is known from the literature that the complete reduction of bulk indium oxide and forming of metallic indium occur in one step. In our previous investigation concerning In_2O_3 loaded on γ-alumina, we have shown that a complete reduction of pure india occurs in one step with a maximum at 755 °C.[50]

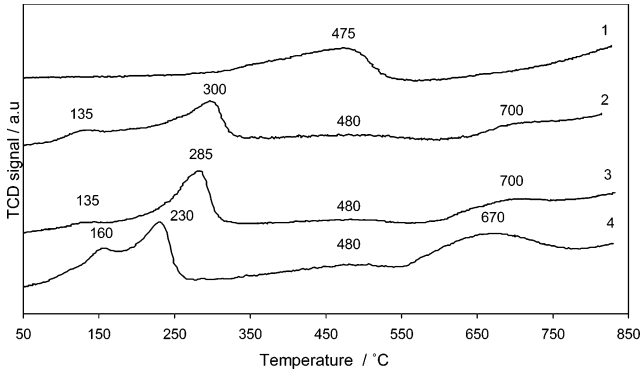

Figure 13. TPR profiles of indium containing samples, obtained in hydrogen atmosphere up to 830 °C: (1) CeO_2, (2) InCe-6, (3) InCe-8, (4) InCe-14. Extents of reduction to In^0: 36.8% for InCe-6; 23.3% for InCe-8; and 20.6% for InCe-14.

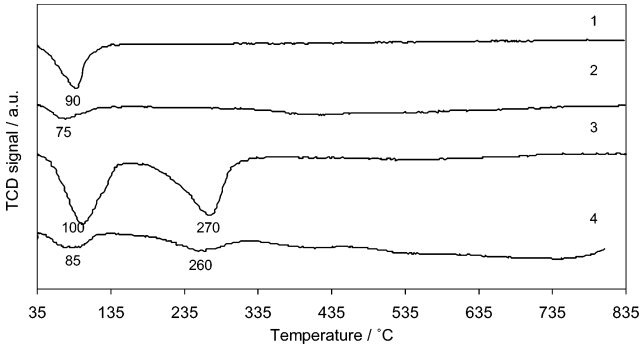

Figure 14. TPO profiles of indium-containing samples oxidized in an oxygen atmosphere up to 830 °C: (1) CeO_2; (2) InCe-6; (3) InCe-8; (4) InCe-14.

In the case of In_2O_3 supported on alumina, two different indium oxide species have been found for compositions containing more than 2.5 wt % indium.[52] In addition, it has been evidenced that the reduction temperature of indium oxide is related to particle size; it has been accepted that the smallest particles are reduced at low temperature.[50−52]

TPR profiles for pure CeO_2 have already been published in the literature.[16,29,44,47,64,71] The reduction of this material happens stepwise, in two temperature regions: lower (350−500 °C) and higher (above 600 °C). TPR peaks found in the lower-temperature region have been assigned to the reduction of surface Ce^{4+} to Ce^{3+}, whereas the peaks at temperatures higher than 750 °C have been attributed to the reduction of bulk CeO_2. Here, the reduction range from RT up to 830 °C was chosen for indium-containing catalysts because the volatilization of In_2O_3 takes place at 850 °C. The obtained results are in agreement with the findings previously stated in the literature.

Figure 13 shows the hydrogen uptakes as a function of temperature for the india−ceria samples with different indium content and that obtained for pure ceria. As can be seen, the TPR profile of pure ceria shows a broad peak at 475 °C, thus proving that the reduction of surface ceria particles from Ce^{4+} to Ce^{3+} happened. In accordance with the literature data, another incomplete peak that started from 600 °C clearly indicates that the reduction of bulk ceria begins only in the temperature region applied for TPR experiments here.

The TPR profiles obtained for $In_2O_3-CeO_2$ present important differences in comparison with pure ceria; all samples containing indium oxide exhibit complex TPR profiles. Three reduction regions can be clearly resolved: a low-temperature one, with two peaks below 400 °C; a mid-temperature region, from 400 to 600 °C, where very weak signals were recorded; and a high-temperature region, where the unfinished reduction processes were noticed.

The doping of indium significantly decreased the peak around 475 °C, which is assigned to the reduction of surface CeO_2. At the same time, the addition of 5.6 wt % In_2O_3 to CeO_2 evidently has as a consequence the appearance of a complex TPR profile with two peaks in the low-temperature region (∼300 °C and a shoulder at 135 °C) and a high-temperature reduction process at ∼700 °C. With increasing the indium oxide loading up to 14.4 wt %, all these peaks shift toward lower reduction temperatures. In accordance with the literature data, the reduction in the low-temperature region proves the existence of well-dispersed india on the surface of ceria. The results presented in Figure 5 prove that changes in the distribution of india particles appear with increasing india content. Besides, the broad reduction peak formed at about 700 °C, which is found for all $In_2O_3-CeO_2$ samples, might originate from the reduction of bulk indium oxide phase, as already stated in the literature.[50] Importantly, the maxima are found at somehow lower temperatures in comparison with the value published in the literature for bulk indium oxide. This fact could be the indication that the presence of ceria can lower the reduction temperature for indium particles in the bulk.

Calculations of the extents of In^{3+} reduction to In^0 and Ce^{4+} reduction to Ce^{3+} were done assuming that the total reduction of In^{3+} to metallic In^0 requires three moles of hydrogen per two moles of indium phase, whereas the reduction of Ce^{4+} to Ce^{3+} requires one mole of hydrogen per two moles of ceria phase. These calculations were done from the integrated peak areas (the baselines were drawn between inset and onset points of each peak). Although some reduction processes are overlapped and others are incomplete, making the integration only partially reliable, the comparison of reduction extents obtained for different samples is still possible. Evidently, the reducibility of indium oxide decreases with the increase of its loading (see Figure 13).

After the TPR procedure was completed, each sample was flushed overnight with helium and TPO was performed in situ. Figure 14 shows the TPO profiles for all the In-containing samples oxidized up to 830 °C. It is worth noticing that the detected oxidation temperatures found below 300 °C are lower than those for reduction.

Bulk cerium samples showed only one peak centered at 90 °C, which can be attributed either to the oxidation of the ceria surface with formation of cation vacancies (O^{2-} or O^-) and /or to the oxidation of Ce_2O_3 to CeO_2. TPO profiles recorded for $In_2O_3-CeO_2$ samples are complex and different among themselves. It is important to point out here that the changes in morphology are caused by the previously performed reduction procedure. As can be seen from scanning electron micrographs recorded for InCe-14 after

(71) Trovarelli, A.; Dolcetti, G.; de Leitenburg, C.; Kašpar, J.; Finetti, P.; Santoni, A. *J. Chem. Soc., Faraday Trans.* **1992**, *88*, 1311.

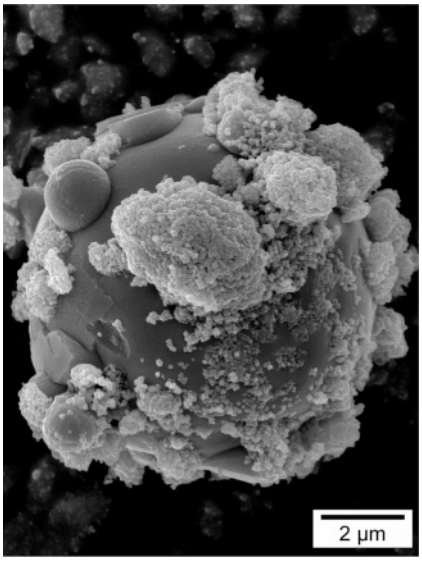

Figure 15. SEM image of the InCe-14 sample recorded after TPR/TPO cycle.

the reduction/oxidation cycle (Figure 15), the existence of spherical particles is visible on the catalyst surface even after the oxidation process; besides, a decrease of up to 90% in the surface areas was observed. Most probably, these particles could be formed by sintering of metallic indium, because this metal can be reduced more easily than cerium. Certainly, this production of spherical particles of metallic indium causes the difficulties in oxidation; moreover, the oxidation is not totally comparable among the investigated samples because of different amounts and different sizes of spherical particles of metallic indium. Still, the obtained results are informative: as can be seen from Figure 14, TPO profiles are dependent on india content. For sample InCe-6, a pronounced peak at 75 °C and a smaller oxygen consumption up to 725 °C oxidation temperature were detected. Sample InCe-8 showed two peaks at 100 and 270 °C with the highest reoxidizing activity among the investigated samples; the second peak can be assigned to the oxidation of the In^0 to In_2O_3.[50] In the case of InCe-14, the TPO profile is similar to the one found for InCe-8 but a lower consumption of oxygen was detected, which can be explained by a higher degree of sintering effect. Importantly, XPS results revealed that the InCe-8 sample has a better dispersion of indium particles on the surface (see Table 1), which could be a reason for prevention of the alloy formation.

To check the influence of the temperature of the reduction/oxidation cycle on the structure and morphology of the samples, one additional TPR−TPO cycle was performed up to 500 °C for InCe-14, having in mind that high-temperature reduction processes of bulk oxides start after 600 °C.

To examine the influence of reduction/oxidation on the structure of In_2O_3−CeO_2 samples, XR diffractograms were recorded after TPR−TPO procedures, which were performed up to either 500 or 830 °C. Figure 16 presents the patterns of pure cerium oxide and that one of InCe-14 calcined at 500 °C in the air. It can be seen that the structure of the calcined InCe-14 sample is very similar to that of pure CeO_2. An identical XR diffractogram has been collected as well after a TPR−TPO cycle was performed on InCe-14 up to

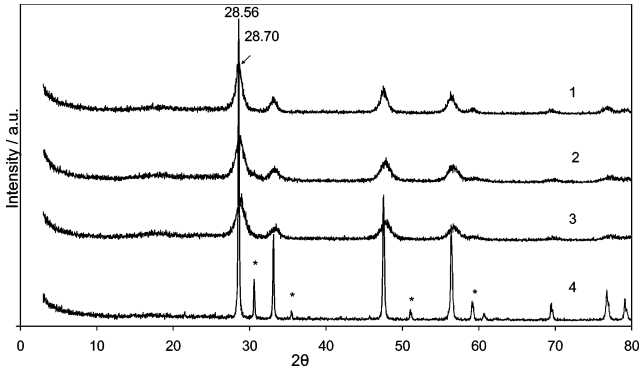

Figure 16. XRD patterns of the CeO_2 and InCe-14 samples collected after different treatments: (1) CeO_2 calcined in air at 500 °C; (2) InCe-14 calcined in air at 500 °C; (3) InCe-14 after TPR/TPO cycle performed up to 500 °C; (4) InCe-14 after TPR/TPO cycle performed up to 830 °C; * = crystal particles of In_2O_3.

500 °C, the same temperature as that chosen for calcinations in air (patterns 1−3). Evidently, reduction−oxidation did not disturb the structure of this mixed oxide. However, the reduction of InCe-14 at 830 °C followed by its oxidation up to the same temperature leads to better crystallization of CeO_2 phase (pattern 4, Figure 16). It is worth noticing that a shift of the main ceria peak toward lower 2θ values (2θ = 28.56−28.70) can be observed. These changes could originate from the already known process of oxygen vacancies generation, which, being a result of high-temperature treatment, produces the changes in a CeO_{2-x} fluorite structure.[22] Importantly, it is visible from the same Figure that In_2O_3 crystal particles appear as a result of these high-temperature processes. Thus, it could be inferred that the reduction/oxidation cycle changes irreversibly the morphology and structure of the samples.

4. Conclusions

The structural, textural, and acidic/basic properties of Me_2O_3−CeO_2 mixed oxides depend importantly on the character of the group III metal. As reported in the literature, the applied coprecipitation protocol allowed relatively high specific surface areas and good homogeneity. All investigated properties seem to be related to the amounts and dispersion of the group III metal oxide. A higher dispersion was achieved for the samples with lower amounts of group III metal oxide.

It can be inferred also that the chosen preparation procedures resulted in true mixed-oxide formulations: the absence of extraneous compounds or mixed phases between ceria and another group III metal oxide is an important feature of all obtained systems. Importantly, the mixed oxides thus obtained exhibit the oxygen vacancies present on the surface of ceria; their concentration has been found to be higher for gallia- and india-containing samples, in comparison with boria−ceria and alumina−ceria formulations. This finding imposes the conclusion that these materials could be active in environmentally important combustion reactions.

The red−ox behavior, investigated only for india-containing samples, has been found to strongly depend on the amount and dispersion of india. The finding that can be very important for possible high-temperature applications is an irreversible change of the structure and morphology of these samples upon high-temperature treatment.

The amphoteric character of ceria, which was already known from the literature, has been confirmed by the results obtained here. However, it is important to point out here that all the other $Me_2O_3-CeO_2$ mixed oxides investigated in this work have also shown amphoteric behavior, in a manner dependent on the character of group III metal. Among the investigated systems, $Al_2O_3-CeO_2$, $Ga_2O_3-CeO_2$, and $In_2O_3-CeO_2$ express somehow more pronounced basic than acidic character. Importantly, $B_2O_3-CeO_2$ samples present an acidic character that becomes more evident with an increase in the boron content. It was observed that the surface basicity comes from Brönsted (mainly) and Lewis sites, whereas the acidity is only of the Lewis type; all these data could be of particular importance for possible catalytic applications.

Acknowledgment. This work was supported by a NATO grant. Special thanks are addressed to Dr. Stephane Loridant, Institut de Recherches sur la Catalyse et l'Environnement de Lyon, for assistance in Raman measurements, and to the technical services of IRCELYON for valuable technical contributions in XRD, BET, SEM, and chemical analysis.

CM062912R